

**High-level Data Fusion Software for SHOALS-1000TH
FY06 Annual Report**

Grady H. Tuell

Optech International
7225 Stennis Airport Drive
Suite 400
Kiln, MS 39556

Phone: (228) 252-1004 FAX: (228) 252-1007 E-mail: gradyt@optechint.com

Steven E. Lohrenz

University of Southern Mississippi
Hydrographic Science Research Center
Department of Marine Science
Stennis Space Center, MS 39529

Phone: (228) 688-3720 FAX: (228) 688-1121 E-mail: steven.lohrenz@usm.edu

Award Number: *W912HZ-05-C-0061*

<http://www.optechint.com> ; <http://www.marine.usm.edu>

LONG-TERM GOALS

Optech International and the Department of Marine Science at the University of Southern Mississippi (USM) have partnered to develop and apply data fusion techniques to combine active and passive remote sensing data for mapping shallow-water and coastal environments. During this reporting period we have: (1) established a collaboration between industry and academia focused on the use of bathymetric lidar and simultaneous passive spectral data for shoreline mapping and characterization; (2) produced a novel paradigm which can be used to formally compare and contrast different strategies for data fusion; (3) developed and implemented 3 high-level data fusion algorithms; (4) disseminated datasets to several other researchers; and (5) worked to understand regional-scale coastal environmental processes through the use of these data.

OBJECTIVES

The objectives of this collaboration are: (1) to develop a number of new data fusion algorithms and computer programs to produce coastal and environmental information from SHOALS-1000TH data; (2) achieve increased accuracy of environmental information extracted from SHOALS-1000TH data through collection and analysis of *in situ* oceanographic ground truth; (3) facilitate the transfer of knowledge from academia to industry regarding the collection and use of *in situ* optical data; (4) facilitate the transfer of knowledge from industry to academia related to application of airborne lidar technology and sensor and data fusion techniques; and (5) facilitate the education of future researchers and workforce through the integration of these concepts into graduate level courses at USM.

APPROACH AND WORK PLAN

To facilitate these objectives, we have worked on the following tasks:

1. Validation and modification of techniques to estimate seafloor and water column properties through the use of coincident *in situ* data.
2. Development of higher levels of data fusion with the SIT fusion model .
3. Implementation of sensor and data fusion strategies for shoreline mapping and land-cover classification.

In the first task, Optech International and USM worked closely with the Joint Airborne Lidar Technical Center of Expertise (JALBTCX) and the National Ocean and Atmospheric Administration (NOAA) to identify a location for a data collection campaign, and to gain access to the CHARTS system. We developed new procedures for acquiring and processing *in situ* data, and acquired new equipment for this purpose. We also developed procedures to share data within the team, and quickly disseminate it to other interested researchers. We scheduled a data collection campaign for the late spring of 2006, but unfortunately, the CHARTS system was not made available. Consequently, a new dataset was not collected and we instead used archived data for the research.

In the second task, Optech International developed and utilized a data fusion paradigm (based on the SIT data fusion model presented in the original proposal) to describe the functionality of data fusion algorithms. Using this paradigm, we developed 3 new high-level data fusion strategies and implemented them in the IDL programming language. These new algorithms accomplish the increasing abstraction of information from data and move from discrete point measurements towards spatial objects.

In the third task, we extended existing and new data fusion concepts onto the beach by combining topographic lidar data with passive spectral data. This work has led to fusion-based land cover mapping, and automated shoreline extraction and characterization. This work has also been coded in the IDL language.

WORK COMPLETED

During this reporting period, we accomplished work in three significant areas: data collection and distribution; development of a data fusion paradigm for high level data fusion; and the development of procedures to auto-extract and auto-attribute shoreline vectors.

1. DATA COLLECTION AND DISTRIBUTION

Optech International and USM personnel collaborated to plan a data collection campaign for the NOPP project. This work consisted of identifying a suitable location; making all necessary arrangements for boat and shore-side support; purchasing and calibrating required instrumentation; development of data processing protocols for the collection and processing of *in situ* data; and the design of the data acquisition scenario for the airborne data. However, due to mechanical problems with the CHARTS system, the government sponsor was unable to provide flight time. For this reason, we initiated research using data from the Optech International archives.

To support similar investigations within the broader research community, we announced the availability of the data at three public venues: the International Laser Mapping Forum (ILMF) in Denver in February; the 7th Annual JALBTCX Coastal Mapping and Charting Workshop in Detroit in June; and at a presentation to the Russian Hydrographic Society in St. Petersburg, Russia, in November. Following these announcements, we received requests for data from 5 researchers (Table 2) and have distributed customized datasets to them. We have also provided all data to personnel at JALBTCX for web-based distribution.

November 2004	CASI-2 passive hyperspectral
July 2005	CASI 1500 passive hyperspectral
November 2004	SHOALS-1000 bathymetric laser
July 2005	SHOALS-3000 bathymetric laser
July 2005 ...	SHOALS 20 kHz topographic laser July 2005
UTM 17 WGS84	
Vertical reference: GPS height above ellipsoid	
Hyperspectral / laser data collected simultaneously	

Table 1. Metadata for the NOPP datasets.

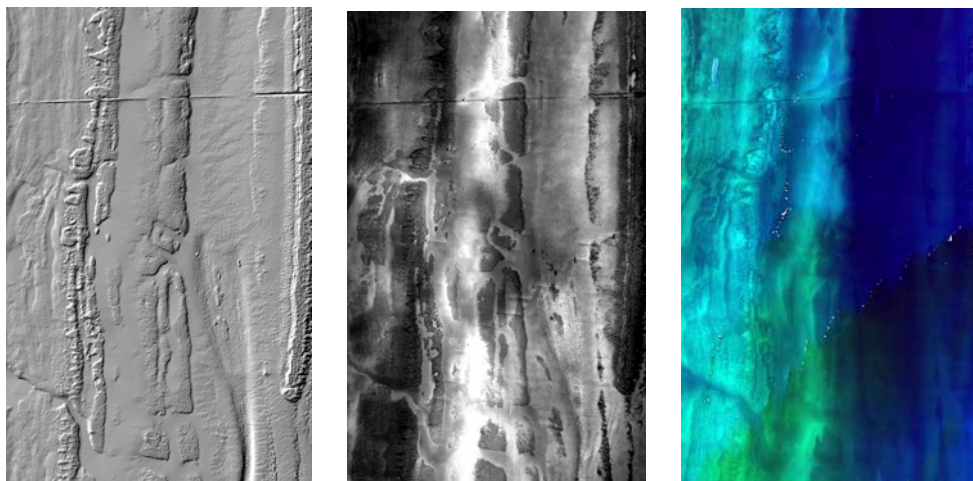


Fig 2. Example of Airborne Data Used in NOPP: Data from 2005 North Block Dataset: SHOALS Depths Shown as Topography (left); SHOALS Reflectance (center); and Casi Surface Reflectance (right).

Name	Affiliation
Dr. ChiQuei Wang	University of Southern Mississippi
Anders Knudby	University of Waterloo
Dr. William Philpot	Cornell University
Dr. Sam Purkis	Nova S.E. Univeristy
Dr. Alan Weideman	U.S. Naval Research Lab

Table 2. Other Researchers Supported with NOPP Data

Unfortunately, the archived data are not well-supported with *in situ* measurements of the water column, and to date, a robust dataset supporting an analysis of optical closure for the airborne remotely-sensed data is not available. Recognizing this, a significant goal of our NOPP collaboration is to acquire a high quality airborne dataset with simultaneous in situ measurements of water column optical properties and seafloor reflectance. Although we were not able to conduct a data campaign during this reporting period, researchers at Optech International and the University of Southern Mississippi (USM) collaborated to identify the types of measurements desired (Table 2). Subsequently, personnel at USM began a systematic effort to acquire and calibrate the necessary equipment, and to develop data processing strategies to produce the desired data from the field measurements.

Measurement	Instrument	Purpose
Water column absorption (a)	AC-9 / AC-S	Evaluate accuracy of (a) estimated from SHOALS and Casi data
Water volume backscatter (b_b)	Eco-VSF3	Evaluate accuracy of (b_b) estimated from SHOALS and Casi data
Water column attenuation (k)	AC-9 / AC-S (absorption) EcoVVF3 (backscatter)	Compare to attenuation derived from CASI and SHOALS data
Water column attenuation (k)	MicroProfiler (integrate irradiance with depth)	Compare to attenuation derived from CASI and SHOALS data
Water column beam attenuation (c)	AC-9 / AC-S	Evaluate the accuracy of (c) estimated from SHOALS data
Water column reflectance (rrs)	MicroProfiler	Evaluate our characterization of CASI water column reflectance
Water-leaving reflectance (rrs)	ASD	Evaluate atmospheric correction and surface correction of CASI data
Seafloor reflectance	DiveSpec	Evaluate quality of seafloor reflectance estimates produced from SHOALS and Casi data.

Table 2. Summary of Desired *In Situ* Measurements.

During this reporting period, researchers at USM developed a protocol for collecting water column *in situ* measurements and developed a vertical water column profiling package using the instrumentation shown in Table 2. The various instruments have been integrated into a single package using the WETLabs, Inc. DH-4 data acquisition system (Figure 3).



Fig.3. USM Instrument Frame With AC-9/AC-S and ECO-VSF3 Being Deployed in Gulf of Mexico for testing (Summer 2006).

Researchers at USM coded algorithms within a Microsoft Excel and Visual BASIC programming environment to enable quick processing of raw data from the *in situ* measurements. These algorithms include integration of optical and CTD measurements, application of various baseline corrections, and the conversion of raw data into necessary formats in geophysical units. The following objectives were addressed:

(1) Application of ac-9/ac-s data corrections

The thermal correction of a/c is performed as:

$$a_{T \text{ corr}}(\lambda) = a_{\text{measured}}(\lambda) - \Psi_T(T_w - 25) - (a_w(\lambda) - \Psi_T(T_{\text{cal}} - 25))$$

$$c_{T \text{ corr}}(\lambda) = c_{\text{measured}}(\lambda) - \Psi_T(T_w - 25) - (c_w(\lambda) - \Psi_T(T_{\text{cal}} - 25))$$

where T_w and T_{cal} are the water temperature during sampling and calibration respectively. $a_w(\lambda)$ is the clean water calibration value. Ψ_T is given (Pegau *et al.* [1]) by:

$$\Psi_T = \sum \{ M_T (M/\sigma) \exp - [(\lambda - \lambda_c)^2 / 2\sigma^2] \}$$

The magnitude, M , width, σ , central wavelength, λ_c , and temperature percentage multiplier, M_T are taken from Table 3 of Pegau *et al.* [1].

The scattering correction on Zaneveld *et al.* [2] is also applied to the unfiltered a measurements:

$$a_{\text{scatter corr}}(\lambda) = a_{T \text{ corr}}(\lambda) - [c_{T \text{ corr}}(\lambda) - a_{T \text{ corr}}(\lambda)] * \{ a_{T \text{ corr}}(715) / (c_{T \text{ corr}}(715) - a_{T \text{ corr}}(715)) \}$$

The absorption and attenuation of pure water at each wavelength can be added as desired. The values for pure water a and c at each wavelength were compiled from published values of Sogandares and Fry [3], Pope and Fry [4], and Buiteveld *et al.* [5].

(2) Processing of VSF3 measurements

The VSF has three sensor heads each providing measurements of scattering at three angles (100, 125 and 150°). Each sensor head operates at a different wavelength, either 440 nm, 532 nm, or 650 nm. A dark calibration of the ECOVSF3 is conducted prior to the start of the experiment to determine the zero offsets of the instrument. This is done by carefully covering a portion of the quartz window over the light detector with electric tape. An average of the dark calibration counts at each angle and wavelength subsequently served as “zero offsets”. Sensor output was adjusted for the appropriate zero offset, and then scaled by a weighting function to provide estimates of volume scattering at each angle.

$$\beta(\lambda) = \text{SF}(\lambda) (\text{raw count}(\lambda) - \text{dark count}(\lambda))$$

where $\text{SF}(\lambda)$ is factory provided scaling factors.

Backscattering coefficients, $b_b(\lambda)$, are estimated by fitting a third-order polynomial to the three values and integrating over angles from π to 2π . Specifically, $b_b(\lambda)$ is computed in the following three steps:

- 1) Multiple $\beta(\lambda)$ by $2\pi\sin\theta$ where $\theta = 100^\circ, 125^\circ, \text{ or } 150^\circ$;
- 2) Fit a 3rd order polynomial to the three measured points and a fourth value equal to zero at $\theta = 180^\circ$;
- 3) $b_b(\lambda)$ is obtained by integrating under the curve fit from $\pi/2$ to π .

A further correction can be made for to correct backscattering measured with the ECOVSF3 for absorption of Twardowski *et al.*, [6]. However, this results in only a minor adjustment for clear ocean waters (VSF3 User's Manual: no attenuation coupling is required for c up to approximately 5 m^{-1}).

(3) Conduct post processing of MicroPro

MicroPro raw files are converted to calibrated geophysical data (Level 1 to Level 2) using the latest version of the Satlantic program ProSoft with raw data files and appropriate calibration files for the instruments as input. Subsequent processing to derive profiles of spectral upwelling radiance (L_u), downwelling irradiance (E_d), and diffuse attenuation coefficient (K_d) are also performed using ProSoft. This program can also compute remote sensing reflectance, R_{rs} . Values of these quantities are as defined in Mobley [7].

(4) ASD processing

An Analytical Spectral Devices, Inc. (ASD) spectrometer will be used to measure *in situ* water-leaving reflectance. It is capable of measuring (1) irradiance (2) radiance. Remote sensing reflectance is calculated by dividing water-leaving radiance by the downwelling total solar irradiance. Thus, the irradiance foreoptic (diffuser) will be placed straight upward to measure downwelling solar irradiance on the ocean surface. In order to measure water-leaving radiance, L_w , we will use the 10 degree field-of-view radiance foreoptic. The measured total upwelling radiance includes some reflected diffuse skylight. This is removed by measuring downwelling sky radiance, estimating the reflected fraction of downwelling sky radiance, and subtracting this from the total upwelling radiance. It is also possible that upwelling radiance is contaminated by sun glint. This contribution is minimized by restricting the azimuthal angle of the measurement to between 90 - 135° relative to the plane of the sun. However, some contribution by glint is still possible and a correction is made for this as well. The relative contributions of the direct solar beam and the diffuse sky irradiance to total solar irradiance will be determined by comparing measured total solar irradiance with that when the diffuser surface is shaded with a small disk.

The computations involved in estimating water-leaving radiance, L_w , are explained below. For (1) optically deep water (2) without the influence of the bottom, L_w is assumed to be near zero in the near IR:

$$L_u = L_w + L_{reflected}^* + L_{reflected}^s = L_{reflected}^* + L_{reflected}^s$$

We can utilize the spectral difference between sky path radiance, L^* , and solar direct radiance, L^s . Thus, we express the total reflected radiance in the IR, L_u , as a linear expression of the unknown relative amounts of the diffuse and direct components:

$$L_u = c_1 L^* + c_2 L^s .$$

Then, the solution is obtained by

$$\begin{bmatrix} c_1 \\ c_2 \end{bmatrix} = \begin{bmatrix} \mathbf{L}^* & \mathbf{L}^s \end{bmatrix}^T \begin{bmatrix} \mathbf{L}^* & \mathbf{L}^s \end{bmatrix}^{-1} \begin{bmatrix} \mathbf{L}^* & \mathbf{L}^s \end{bmatrix}^T \mathbf{L}_u$$

2. Development of High-Level Data Fusion Algorithms for Bathymetric Lidar and Spectral Data

The main goal of this NOPP project is to develop sophisticated strategies for combining airborne remotely-sensed data for the purpose of mapping and monitoring the coastal zone. In the initial proposal, we advocated for the adoption of the SIT model as a data fusion paradigm, and discussed how it might be used to compare different approaches of combining active and passive data. The SIT model is unique because it describes the progression of a series of connected data processing modules leading to increased levels of abstraction in three domains: the spatial domain (wherein data are abstracted into objects); the information domain (wherein data are abstracted into identities); and the technique domain (wherein increasingly abstract and complex algorithms are employed).

We show the SIT concept in Figure 3(a). Over the past year, researchers at Optech International have advanced the original SIT model by combining and adding fusion levels in the spatial and information domains. We illustrate the amended model in Figure 3(b). Here, the dotted line leading to $I_{x,y,z,t}$ indicates our desire to move to the highest levels of abstraction along both axes, with the ultimate goal of producing information about objects in the spatial domain at the time of observation. Here, we note the term feature is used on both axes. The SIT model resolves the ambiguity related to its dual use, and allows for the description of recursive and iterative processes.

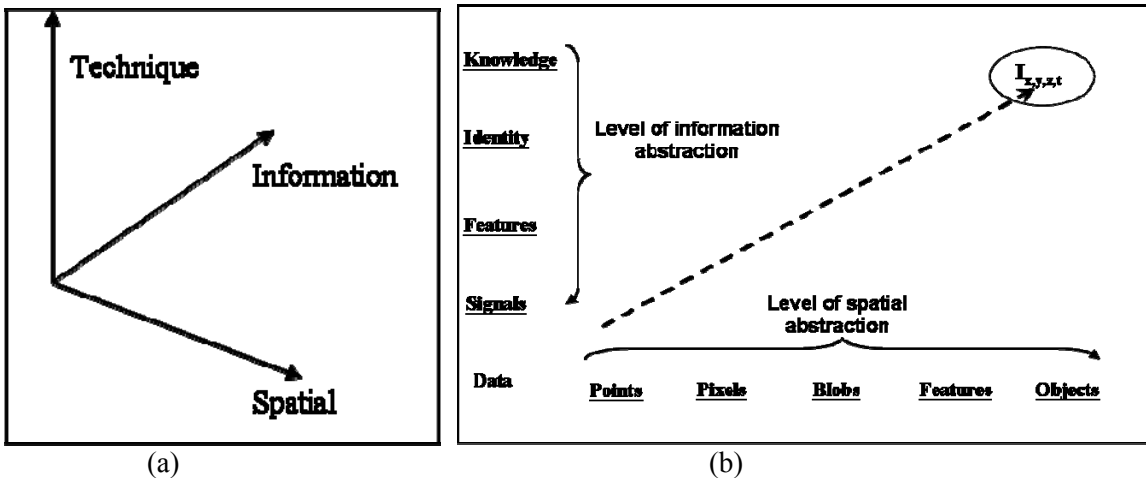


Fig. 3. The SIT Data fusion Model, (a) 3D SIT concept, (b) Spatial and Information Axes of SIT Model.

The SIT model can be used to describe complicated procedures with a simple graph. For example, one possible strategy for classifying the seafloor with SHOALS data alone is to use a Maximum Likelihood Classifier on a multi-dimensional feature space of texture metrics extracted from Gray Level Co-occurrence Matrices. This procedure requires the computation of calibrated SHOALS waveforms at correct spatial coordinates; the estimation of depth, attenuation and reflectance from each waveform; the rasterization of the discrete point values into a spatial image; and the subsequent extraction of texture metrics and classification of individual pixels.

This procedure encompasses the evolution of raw SHOALS data into spatial pixels and information. In Figure 4, we use the SIT model to illustrate it. Here, the numbered triangles represent individual data processing procedures, and the oval indicates the culmination of the process with an identity declaration for each pixel.

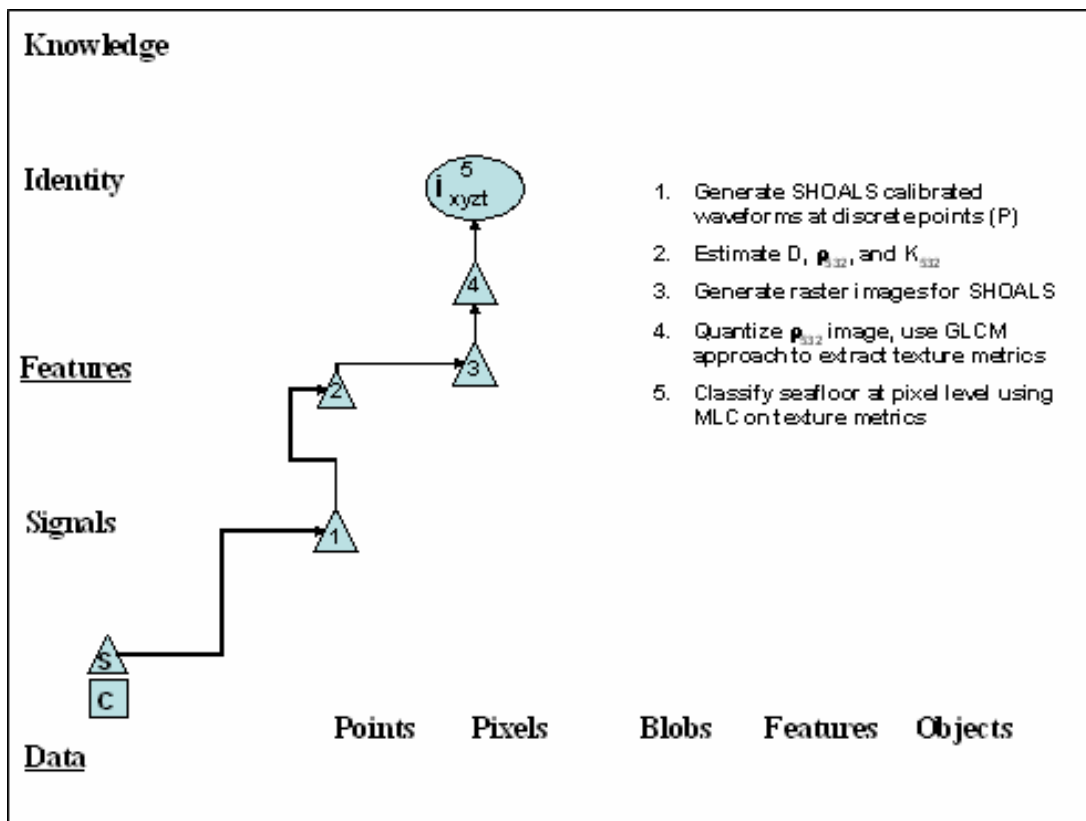


Fig. 4. SIT Model Used to Illustrate Seafloor Classification with SHOALS Data

The value of the SIT model is realized when one has the requirement to understand and compare more complicated procedures. For example, researchers at Optech International have developed algorithms to achieve an inversion of the radiative transfer equations for a passive spectrometer using the depth, attenuation, and reflectance estimated from SHOALS data as constraints [8]. This procedure leads to estimates of seafloor reflectance in the individual spectral channels of the passive imager, and ultimately to the use of spectroscopic techniques for classification of the seafloor from the spectral data.

We illustrate this process in Figure 5. Here, the triangles represent algorithms operating on the SHOALS data, and the squares represent algorithms operating on passive spectral imagery acquired by using a Casi instrument. The combined symbol at step 7 indicates a data fusion step, where the inversion of the imaging equations for the spectrometer is accomplished using lidar depth, reflectance, and attenuation as constraints. Finally, at step 8, an identity declaration is achieved for each pixel of the once-fused data.

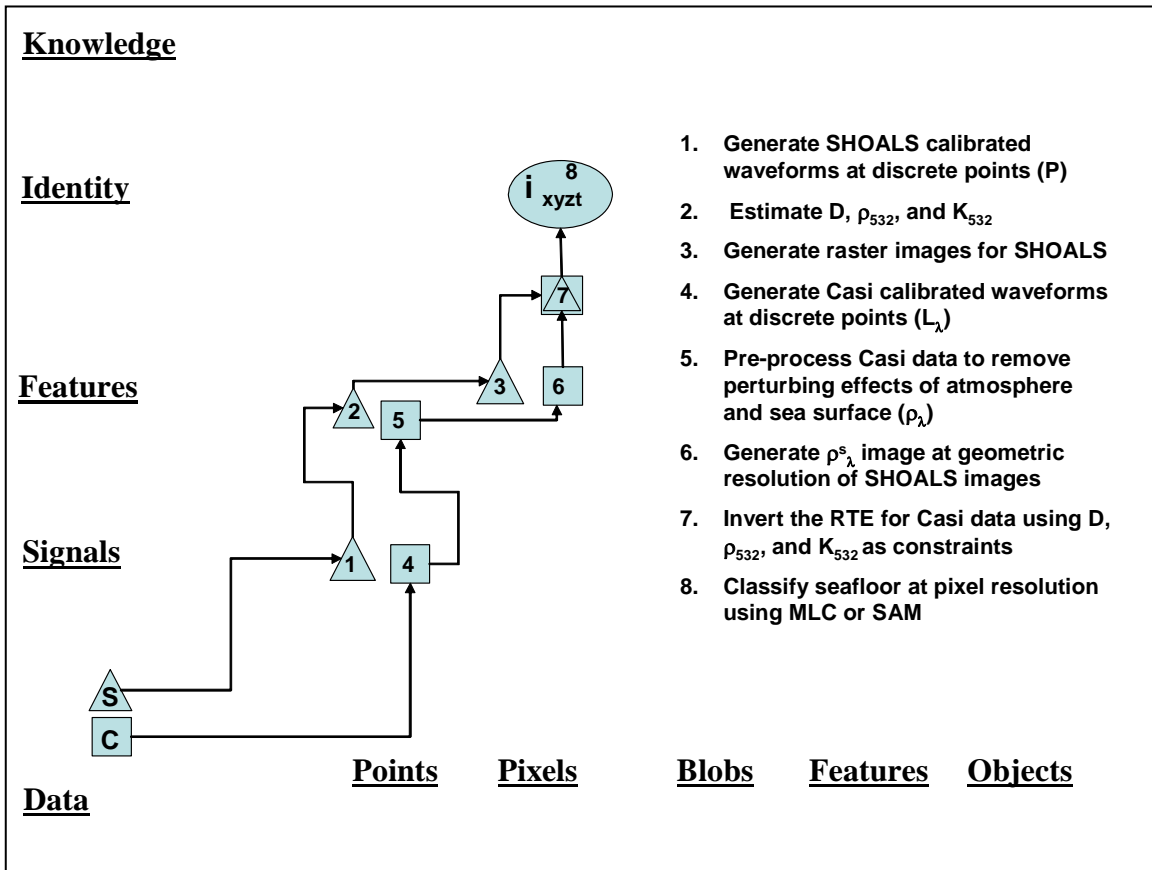


Fig. 5. SIT Model Used to Illustrate Seafloor Classification in a Data Fusion Paradigm

Comparison of Figures 4 and 5 allows one to quickly ascertain the basic evolutions of the data and to compare a lidar only procedure to a procedure based on data fusion. It allow indicates an important result: the two procedures lead to separate classifications of the seafloor. We now ask a new and critical question: what do we do if the two classifications do not agree? We believe the answer lies in the consideration of higher levels of data fusion on the information axis. For this reason, we extended our earlier definition of the information axis (as shown in the original proposal) to include a higher-level state, *knowledge*.

We define *knowledge* as a state of information where we have resolved a conflict arising from disagreement of the individual identity declarations. Over the past year, we have worked to achieve

a state of knowledge by combining individual classifiers using Dempster-Shafer evidential theory [9]. This theory resolves the ambiguities by combining probabilities from the initial identity statements. We illustrate this higher-level procedure in Figure 6. Here, steps 5 and 10 represent the individual identity statements shown in Figures 4 and 5 respectively, and step 11 represents the state of knowledge achieved through use of the Dempster-Shafer process.

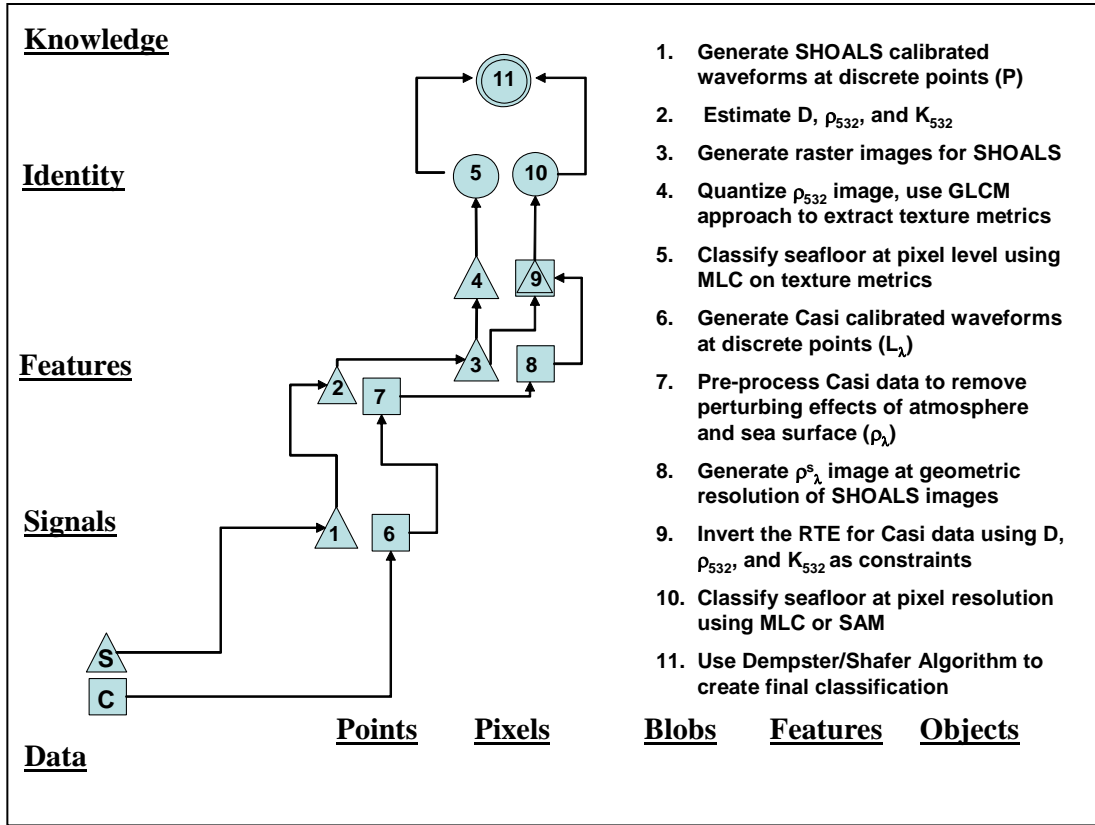


Fig. 6. SIT Model Used to Illustrate Higher-level Fusion Achieved with Dempster-Shafer Algorithm.

In Figure 7, we show the three classification maps. The classification in 7 (a) was produced using the procedure shown in Figure 5. Here, a large attenuation boundary in the water column (clearly visible in Fig. 2) has not been completely compensated in the constrained inversion, and leads to a misclassification of the seafloor in the lower right part of the image. We performed an accuracy assessment using ground truth provided by personnel at the National Coral Reef Institute of Nova S.E. University (NSU), and determined the overall accuracy to be 61%. In 7 (b), the classification was produced from SHOALS data alone using the procedure illustrated in Figure 4, and the overall accuracy is 69%. In 7 (c), we have combined the initial classifications using the process shown in Figure 6, and this procedure yielded an overall accuracy of 89%. Because the classification images are co-registered to the depth data, we may easily produce a 3D classification map as shown in Figure 8.

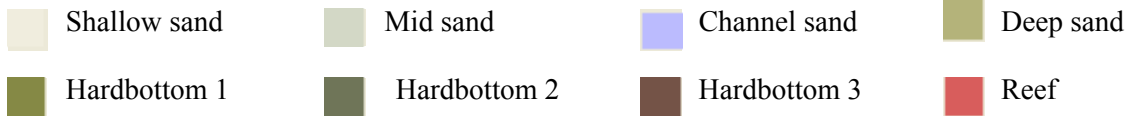
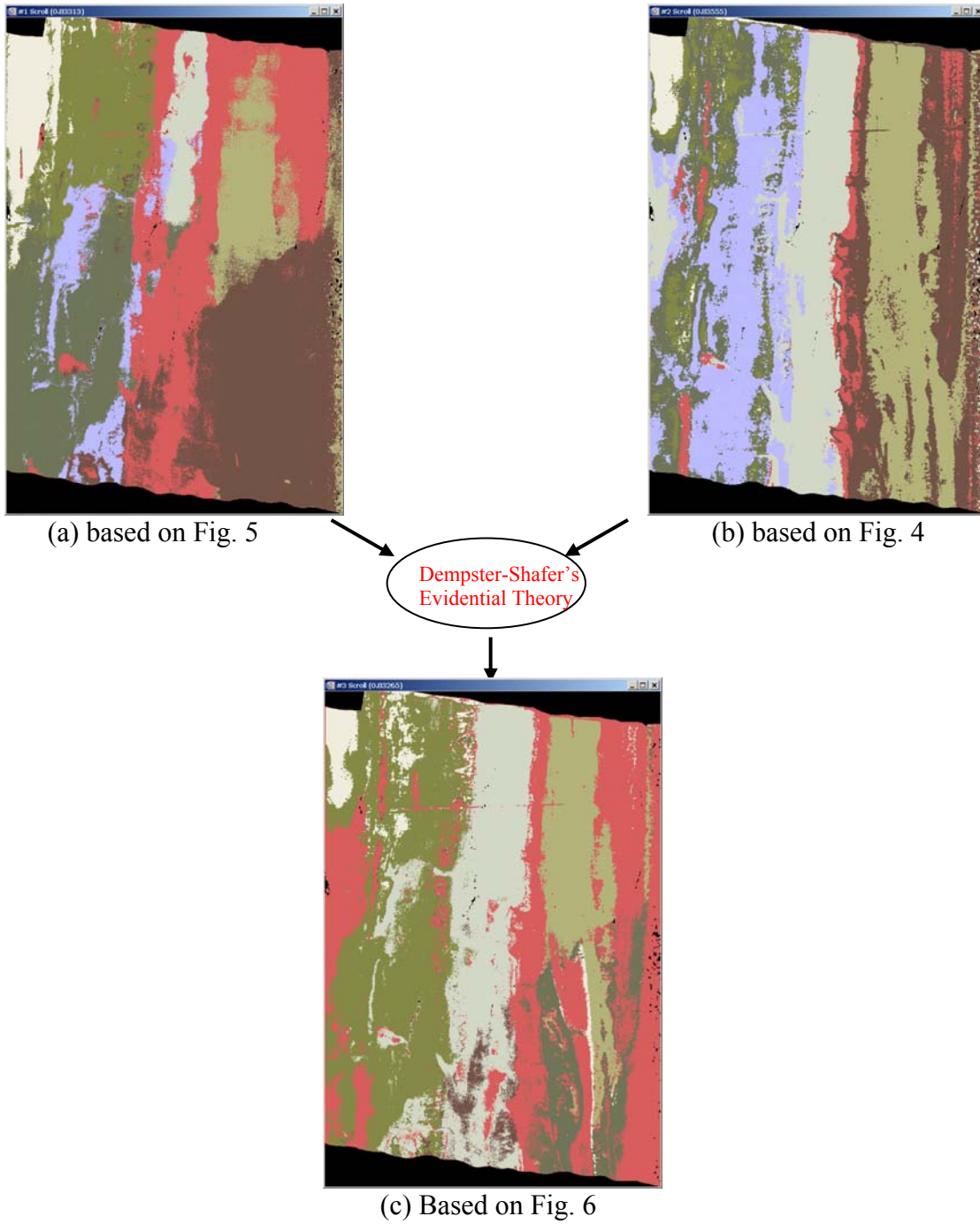


Fig. 7. Classification Maps Produced Using the Procedures Shown in Figs. 4, 5, and 6.

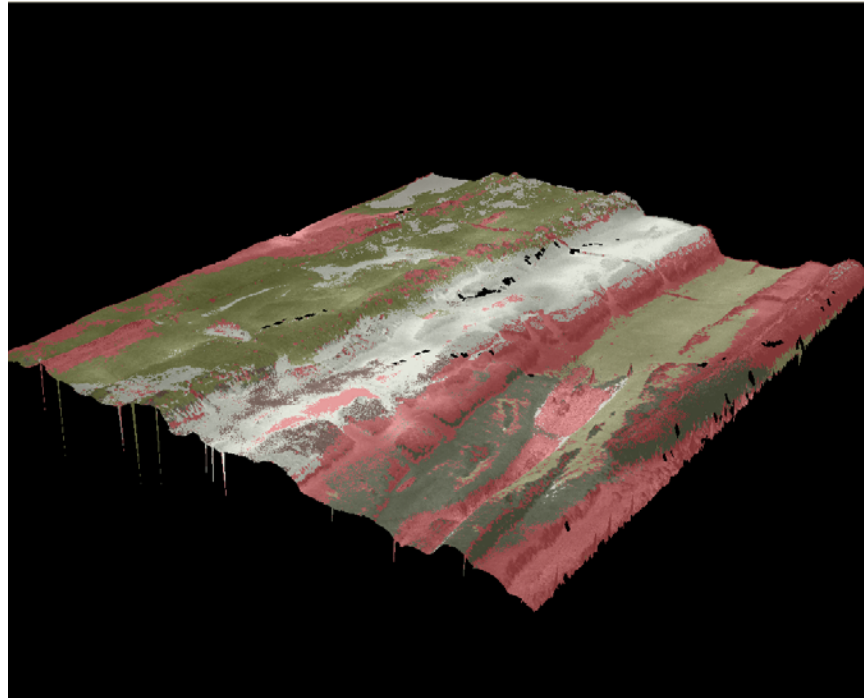


Fig. 8. 3-D sea floor pixel-level classification image

These encouraging results support the original hypothesis that higher-level fusion on the information axis leads to higher classification accuracies. However, there has been no equivalent increase in the level of abstraction on the spatial axis. This increase must be achieved by considering spatial groupings of similar pixels to create blobs. A blob is defined in the computer and robot vision community as a region or group of connected components [10].

We implemented a connected components operator to create spatially contiguous blobs from individual classified pixels. We show this procedure at steps 11 and 12 in the SIT data fusion model in Figure 9. Once the blobs are created, we invoke set theory to intersect the blobs, and pass the prior probabilities from the pixels to the blobs so that we may apply the Dempster/Shافر process at step 13. To make this work, we computed prior probabilities for each blob by averaging the probabilities for the pixels within each blob.

To illustrate these results, we show in Figure 13 (a) and (b) the blob images created from the Casi and SHOALS pixel classifications, and in (c) the intersected blobs. Here, the color scheme is used to indicate the presence of discrete blobs and should not be confused with colors used previously in the classification scheme. We also note the large number of blobs in (c). Our analysis revealed about 70% of the intersected blobs represented conflict (the SHOALS blob did not agree in classification with the Casi blob) clearly indicating the need for implementation of a higher-level process on the information axis.

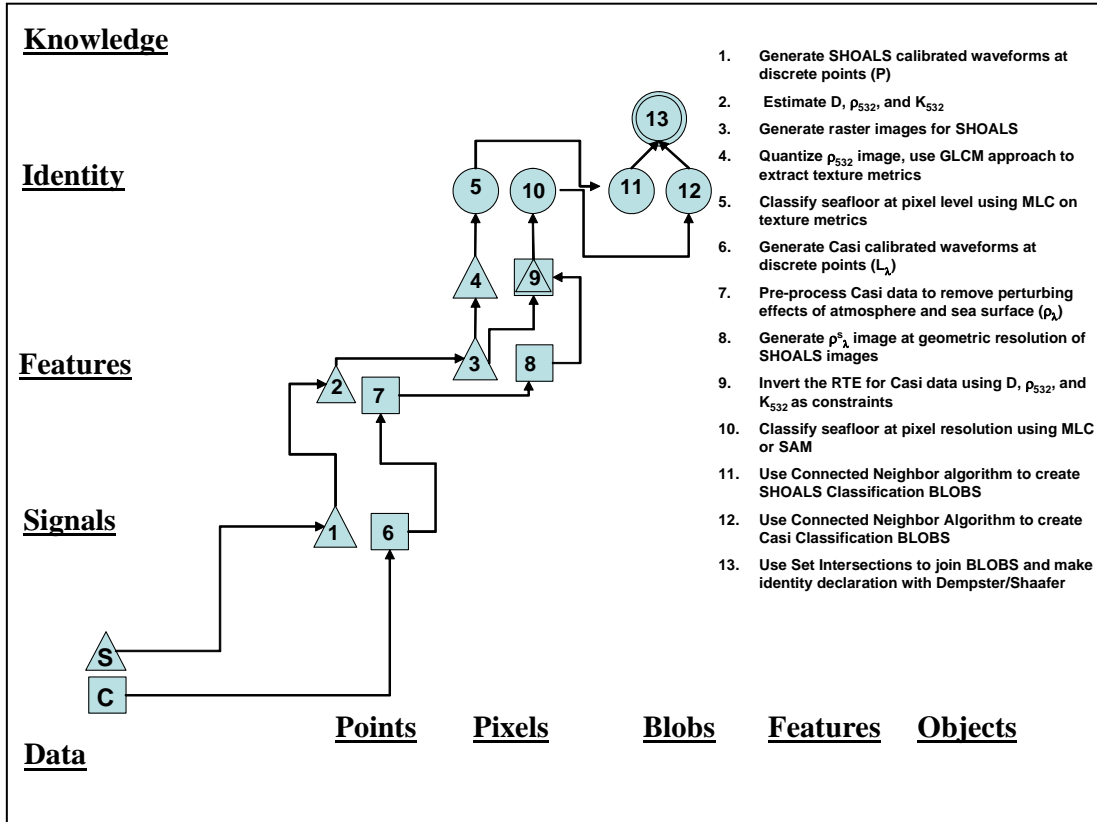
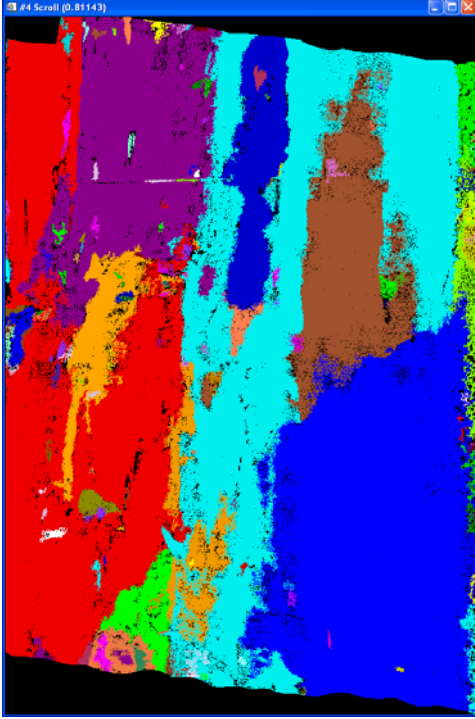


Fig. 9. Illustration of Higher-level Fusion on Both Information and Spatial Axes of the SIT Model

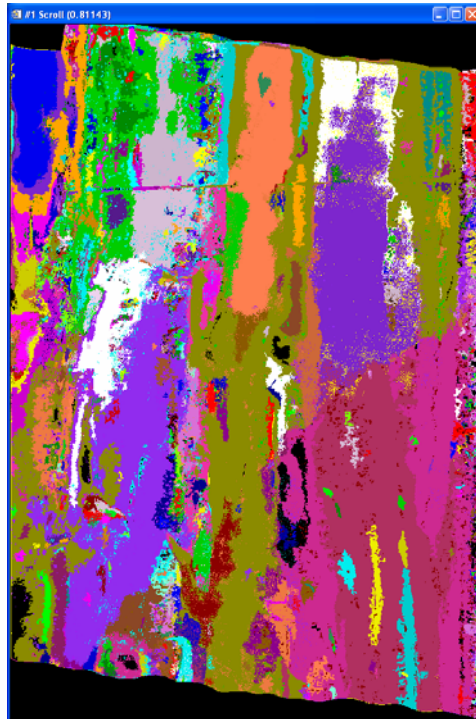
These results shown in Figure 11 are preliminary and are shown here only to illustrate progress towards the project goals. The blob-level fusion image generally looks to be a better classified image, but we have not fully resolved the processes of creating probabilities and propositions for the blobs, as required in the Dempster/Shafar algorithm, and make the process autonomous. Also, we are experimenting with alternative techniques for estimating probabilities from the Maximum Likelihood Operator.



(a) CASI Blob Image (183 blobs)



(b) SHOALS Blob Image (362 blobs)



(c) Intersected Blob Image (1199 blobs)

Fig. 10. Blob images with 8-connectivity and 5 pixel minimum blob size.

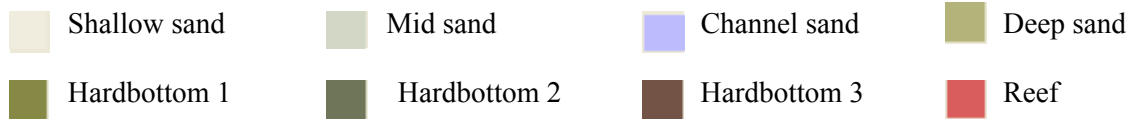


Fig. 11. Blob-level Classification Produced Using Procedure Shown in Figure 9

3. DEVELOPMENT OF DATA FUSION ALGORITHMS FOR TOPOGRAPHIC LIDAR AND SPECTRAL DATA

The SHOALS-T bathymetric lidars produce topographic data when flown over the beach. Many users of bathymetric lidar data in the U.S. government are interested in shoreline studies and the combination of bathymetric and topographic lidar data is ideal for this purpose. For this reason, we have worked to develop auto-extraction and auto-attribution tools for shoreline and land-cover applications.

Researchers at Optech International have developed a preliminary capability to produce land reflectance images at 532nm from the APD channel of the SHOALS lidar. We also developed techniques to boresight the CASI passive imager to these reflectance images. This procedure

produces a dataset containing heights, depths, SHOALS reflectance images, and a datacube of passive spectral reflectance computed by performing atmospheric correction of the airborne radiance data.

The SHOALS land reflectance images are a novel product developed in this project. To compute them, we estimate reflectance from each calibrated waveform by isolating the timebin at the halfpower point of the surface return, as shown in Figure 12. We then normalize the SHOALS time resolved digitized waveforms (Fig. 13) using a set of regression equations obtained during the calibration of SHOALS system.

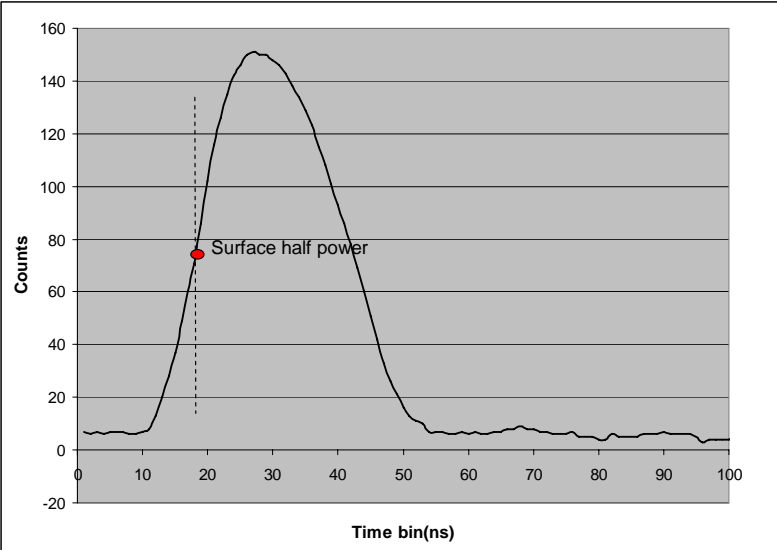


Fig.12. A typical APD land return in the electrical domain.

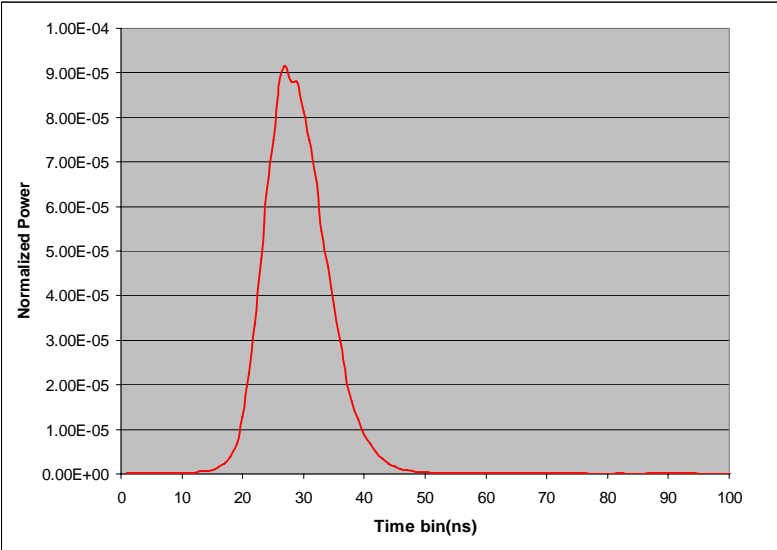


Fig. 13. Normalized APD waveform.

We then compute the land reflectance as:

$$\rho_{land} = \frac{A_r \cdot P_t \cdot 2P_{surface}}{\pi(H / \cos \theta)^2 \cdot \cos^2 \theta \cdot e^{2(c_A)H / \cos \theta}}$$

where, ρ_{land} is the absolute reflectance and $P_{surface}$ is the SHOALS surface half power.

c_A Is the atmosphere “attenuation”

H Is the aircraft altitude

P_t Is the transmitted power

To support the development of algorithms for shoreline mapping, we generated the beach zone image shown in Figure 14 by rasterizing the individual values of reflectance. Investigation of the pixel values in this image reveals the PMT channel often saturates over land. Also, there is an indication we ought to perform radiometric calibrations of the system at different background levels so that we can better compensate for changes in solar background at 532nm. These points indicate the need for further research. Never-the-less, preliminary analysis of the accuracy is encouraging. For example, we show in Table 3 that the SHOALS reflectance agrees well with values measured with a hand-held spectrometer over three landcover types, and they also agree well with values computed from the Casi airborne spectrometer.

Easting	Northing	Reflectance (%)			Description
		ASD	CASI	SHOALS	
2873448	588260	30	26	26	Beach Sand
2873437	588234	13.5	14	12.7	Green Tennis Court
2878056	588169	5	9	9	Grass

Table 3. Comparison of Reflectance Values Measured with SHOALS, Casi, and ASD

One routine but challenging task in the processing of airborne passive spectral images is the boresight alignment of the imager. The boresight alignment computes the offsets from the individual components of the navigation system to the imaging sensor head. The computation is essentially a coordinate transformation requiring the measurement of a number of points on both the images and the ground. The required ground control point measurements can be expensive and difficult to acquire. In this project, we developed a procedure to use SHOALS reflectance images (Fig. 14) in lieu of ground control to accomplish this task. This process has subsequently proved to be effective and efficient, and yields images of the type shown in Figure 15.

To check the accuracy of the spatial coordinates of the derived Casi images, we compared the image to ground points surveyed using GPS techniques and determined the average errors in horizontal coordinates to be less than one pixel in both coordinates.



Fig. 14. Reflectance image generated using the APD channel



Fig. 15. CASI-1500 hyperspectral imagery (left) and topographic laser elevation data (right) with extracted ground control points (+). Data acquired over Hallandale Beach, Florida, July 2005. These data are available through NOPP.

Using the co-registered SHOALS lidar and Casi spectral data shown in Figure 15, Dr. George Raber of USM has developed high-level data fusion algorithms to accomplish land-cover classification and auto-extraction and auto-attribution of shoreline vectors. This work has been accomplished wholly under this NOPP project, and in collaboration with Dr. J.Y. Park of Optech International.

The procedure to accomplish topographic classification combines several innovations. For example, in the SIT model in Figure 16 we see in Step 7 a mean-shift algorithm is used to segment the Casi image into blobs. These blobs represent spectrally homogeneous areas within the Casi reflectance images (Figure 17).

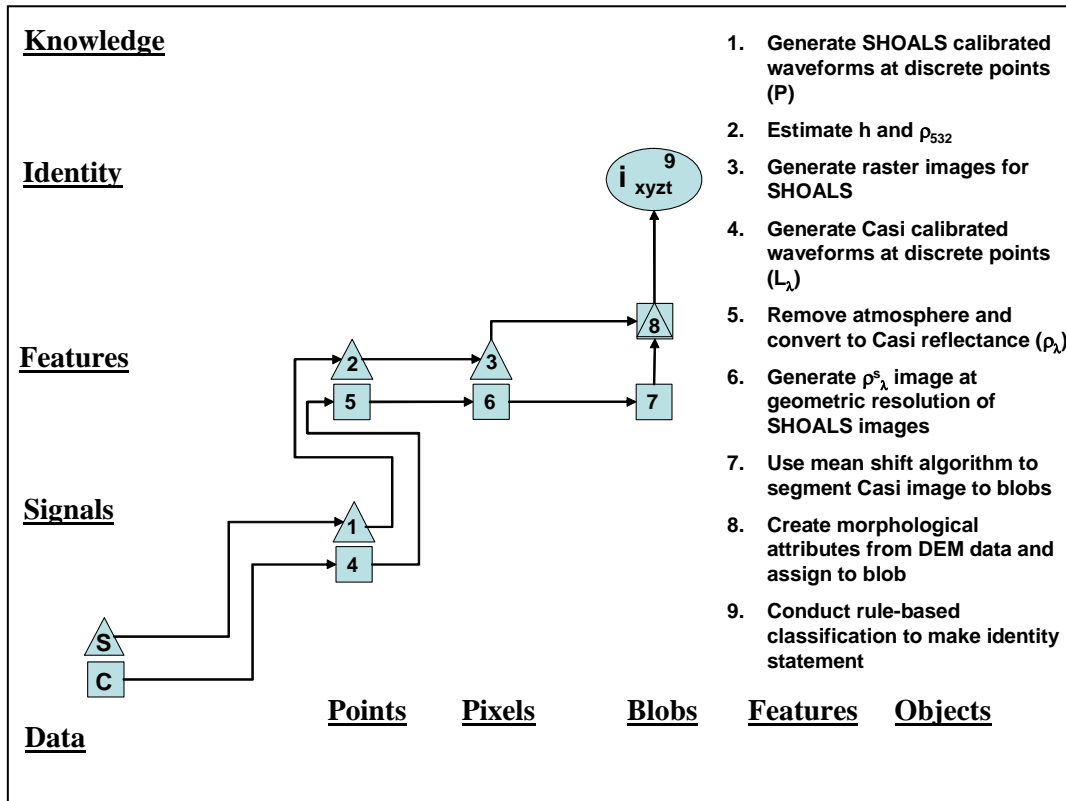


Fig. 16. SIT Model Illustrating Rule-based Topographic Classification



Fig. 17. Topographic Blobs Produced from Casi Data with Mean Shift Algorithm

The lidar data within these spatial blobs are subsequently used in step 8 of Figure 16 to extract and attribute several morphological features (Table 4) to the blobs as demonstrated in Figure 18.

	Description
Shape Statistics	Area, Perimeter, Compactness, Fractal Dimension
LIDAR Basic Statistics	Mean, Median, Range, Portions of the Mean and Range (e.g. 10% to 90%), Standard Deviation, Skewness, Kurtosis
LIDAR Vertical Distribution Statistics	Vertical Histogram of Z values, Cumulative histogram normalized to 1.
LIDAR Spatial Autocorrelation Statistics	Empirical Semi-variance calculated at a number of different lag values.
LIDAR Curve fit Statistics	The residual is calculated for fitting a 1st – 5th order polynomial curve through the segments z values.
Hyperspectral Data Statistics	Mean, Range and Mean of the middle 80% of the data are calculated.

Table 4. Morphological Descriptors Assigned to Blobs

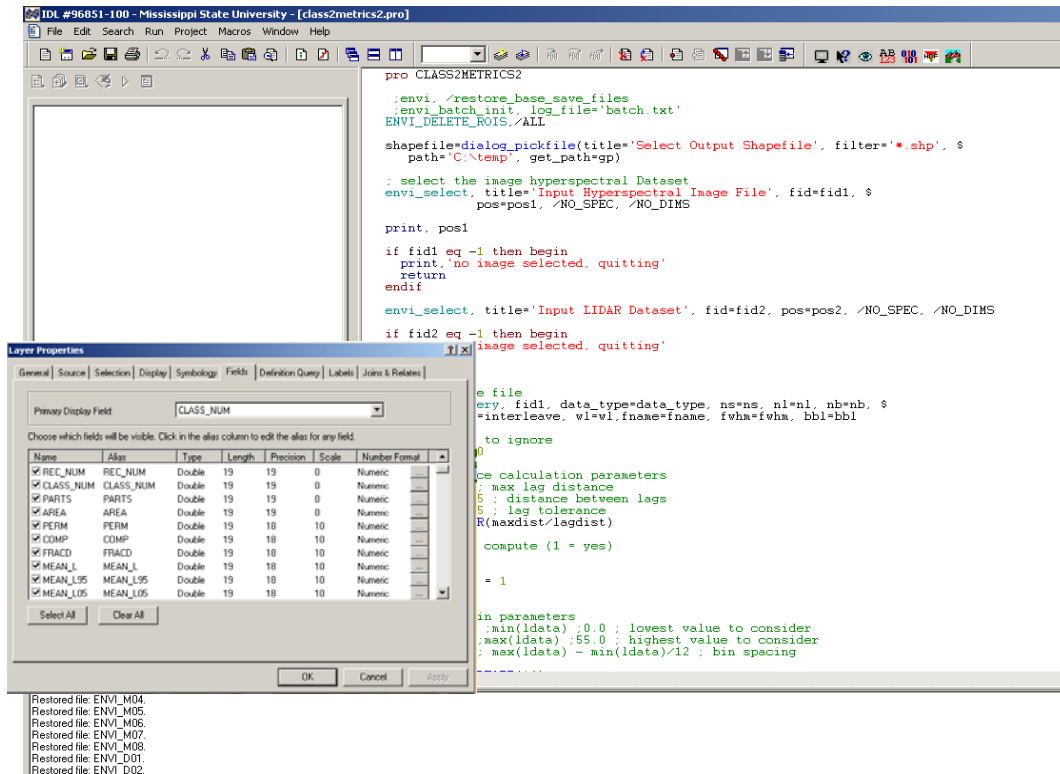


Fig. 18. IDL code for the attribution of the image segments with the segments listed in an ESRI dialog.

The blobs are eventually classified in step 9 with a rule-based technique. The required rules are created using an automated rule generator to analyze training data specified by the user for each land cover class. We show an example decision tree structure generated for this project in Figure 19.

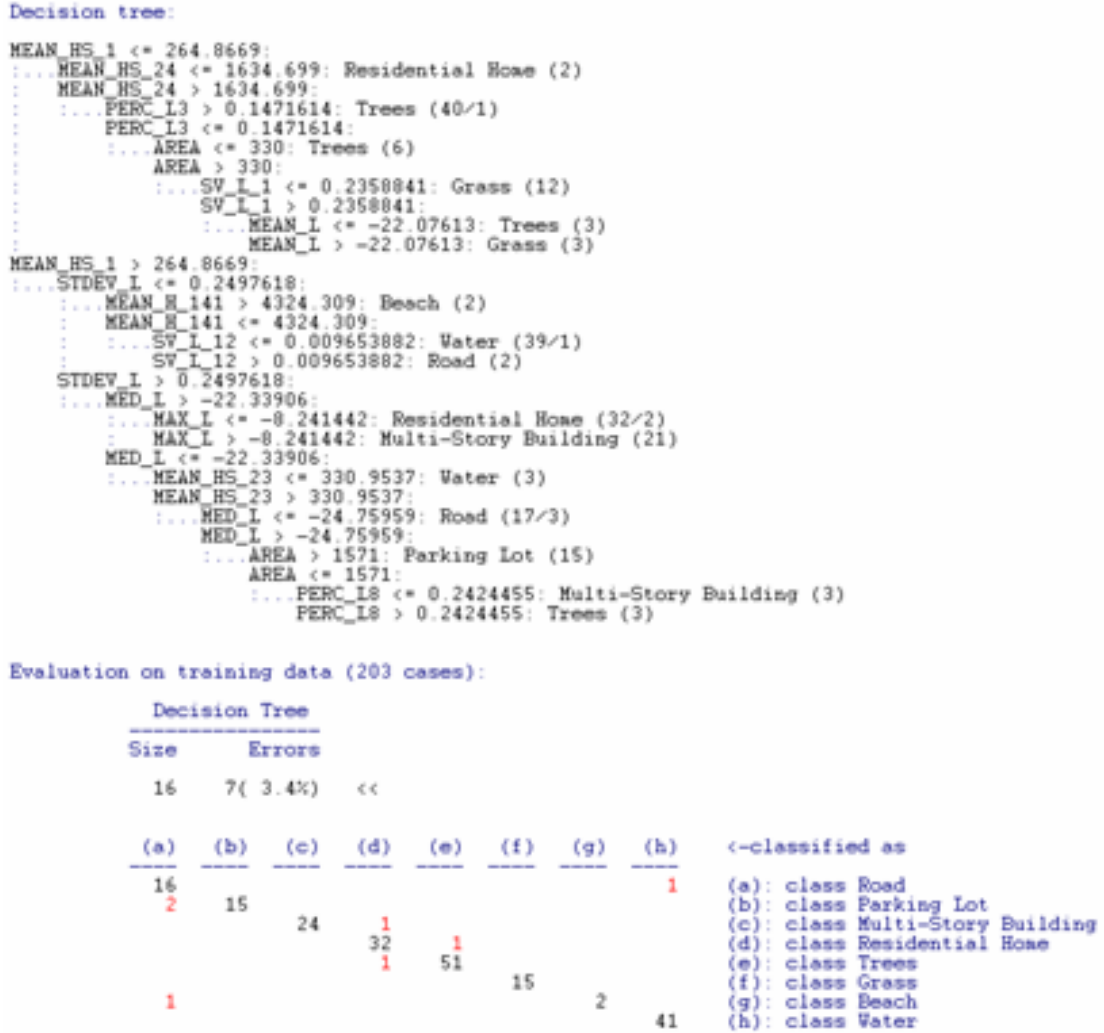


Fig. 19. Decision Tree Used to Accomplish Topographic Classification

In Figure 20, we show a preliminary topographic classification achieved using the SIT model shown in Figure 16, and a color composite image of the Casi hyperspectral surface reflectance data. The classes used are not part of an accepted classification scheme, but were selected to facilitate the development of the procedure. The resulting classification is approximately 80% correct when analyzed using a subset of training data withheld for this purpose. The largest misclassifications occur in heavily shadowed areas.



(a) False-color Composite from Spectral Data



(b) Topographic Classification

Fig. 20. Illustration of the Topographic Classification Procedure Shown in Figure 16

The combined topographic and hydrographic data produced by the SHOALS lidar can be used to generate a seamless 3D dataset of the beach and shallow water seafloor. Consequently, geometric shoreline vectors can be auto-extracted from the data as contours of the appropriate height, and the resulting line segments can be subsequently intersected with the topographic classification map to accomplish an auto-attribution of the shoreline vector.

We have created a procedure to accomplish auto-extraction and auto-attribution of shoreline vectors. This procedure requires 4 inputs:

- a classification map of the beach area
- a DEM derived from SHOALS data that includes both underwater and land elevation values.
- a file containing locations of NGS Tide Gauges with offset to desired vertical datum (e.g. MLLW, MHW)
- a parameter file supplying smoothing factors for each class type.

Using the tide station data, we convert the height values in the DEM to the datum of interest, and extract the contour. Because the height data can be noisy, and the DEM usually contains voids caused by missing depths in the hydrographic survey data, we apply spatial smoothing techniques to the height data prior to extraction of the contour. We then select the longest contour to represent the shoreline. The shoreline vector is then intersected with the classification image, and a one-dimensional smoothing is performed on the vector to generate a more visually appealing cartographic feature. The vector is subsequently subdivided and attributed with the classification type, and the final result is stored as an ESRI shapefile. This procedure is implemented entirely in IDL/ENVI, and does not rely on any external programs. We have conducted preliminary tests of the procedure using the Fort Lauderdale data.

We demonstrate test results in Figures 21, 22, and 23. For this test, we used a datum conversion from WGS84 (ellipsoid height) to NAVD88 (orthometric height) of 28.1 feet, and extracted a NAVD88 shoreline vector. Within the study area, only one landcover class (beach) exists along the coast. In order to demonstrate the adaptive smoothing and auto-attribution capabilities, we arbitrarily introduced an additional class.

In Figure 21, we show the auto-extracted, auto-attributed NAVD88 shoreline on a gray scale image of the DEM. Here, the orange and magenta sections of the vector represent different shoreline attributes. In Figure 22, we show a detail view of the vector, and illustrate the application of different amounts of spatial smoothing applied to the different shoreline attributes. Finally, we show in Figure 23 the resulting shoreline on a color composite image generated from the Casi spectral data.

Several members of the research team recognize the challenges associated with production-level implementation of shoreline mapping. The results shown are promising, but are only a beginning. The procedure must be made more robust to handle complicated shorelines, and it must be tested with other datasets. Also, we must decide upon and implement a topographic classification scheme for the initial classification that permits a useful auto-attribution of the shoreline segments.

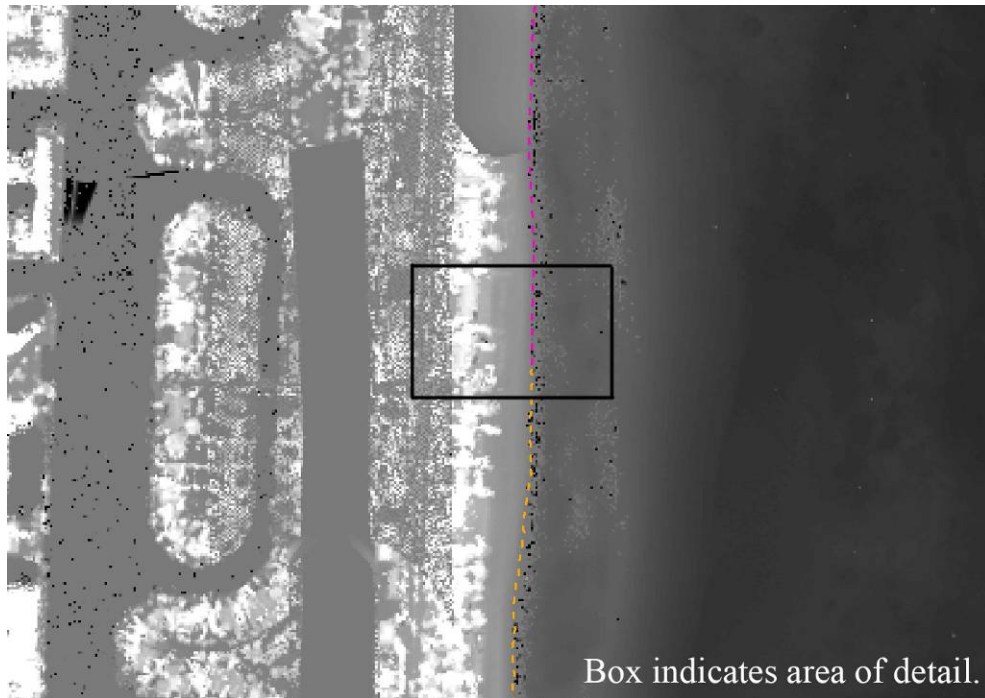


Fig. 21. An overview of the auto generated shoreline on top of the shoals DEM. The boxed area indicates the area of detail for the next two figures.

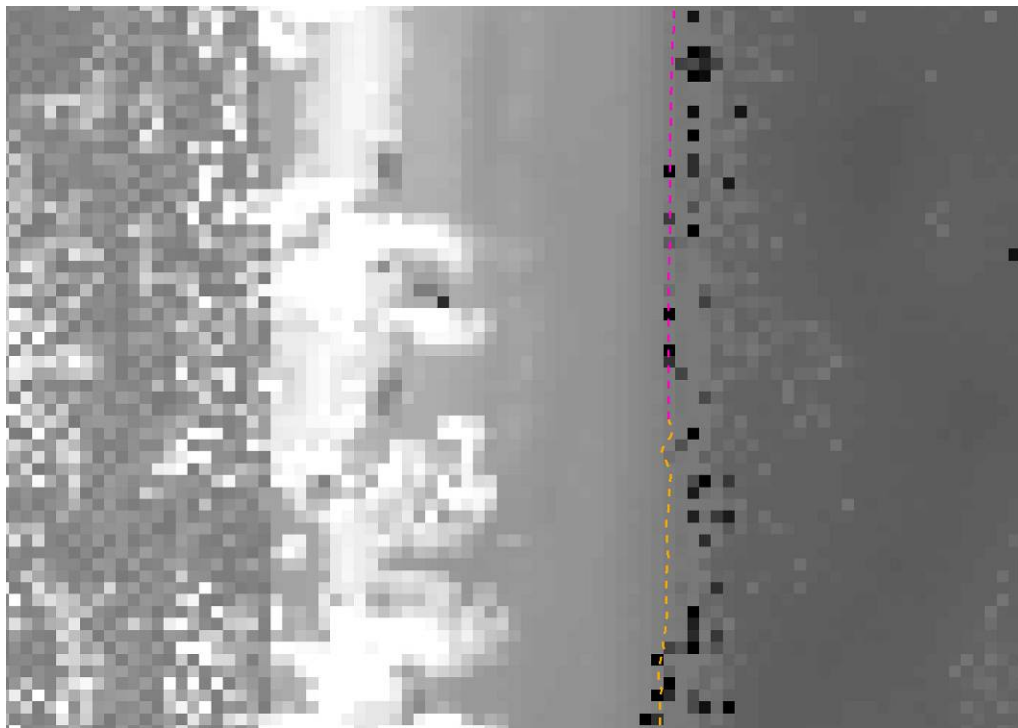


Fig. 22. A detail of Fig. 21. Note the magenta line has been smoothed more than the orange line.

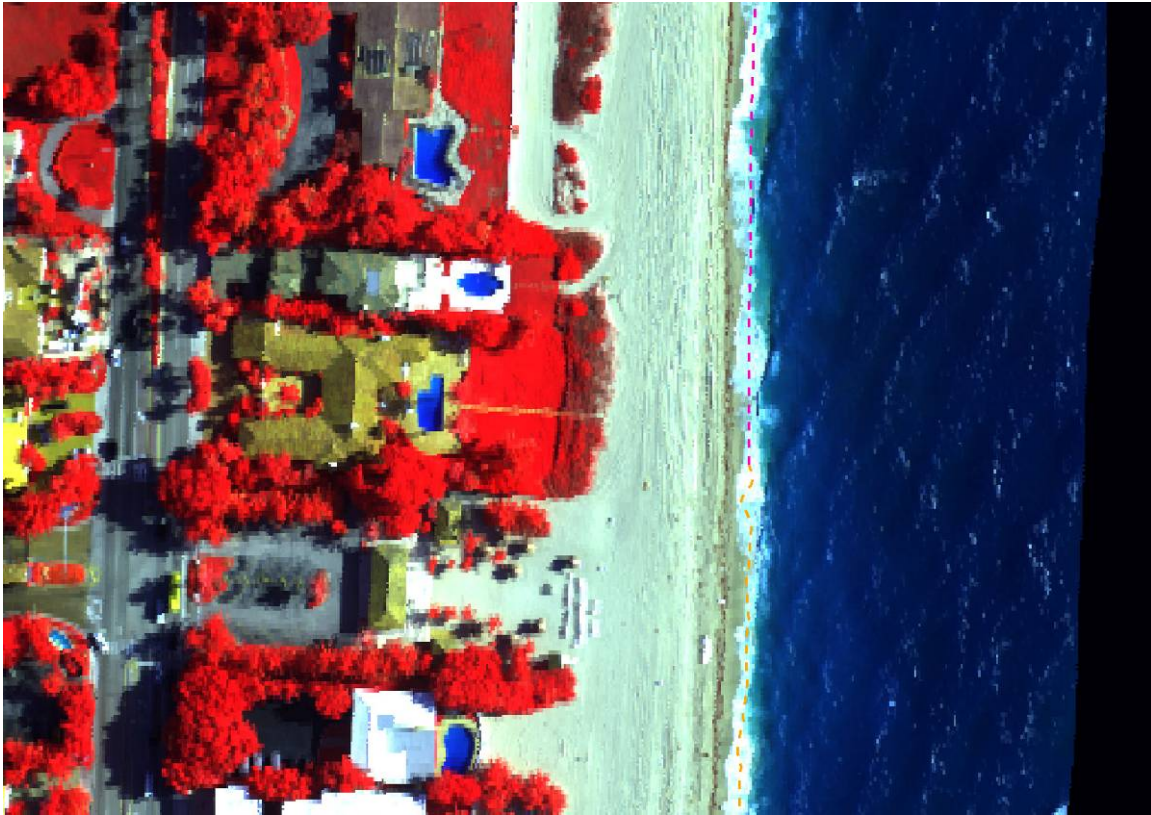


Fig. 23. Shoreline vector depicted on a color composite of the hyperspectral data. The area is the same as Fig. 22.

RESULTS

During this reporting period we have produced significant results in three aspects of the project: data collection and dissemination; refinement of the SIT model for describing and analyzing data fusion procedures; implementation of several high-level data fusion procedures; and the implementation of a data fusion strategy for auto-extraction and auto-attribution of shoreline vectors.

We organized and fully processed several datasets from Optech International's data archive (Table 1) and subsequently used these data to support the research goals of this project. We also shared these data with several other researchers (Table 2), and made them available on the web. We acquired new optical equipment for the measurement of water column insitu data (Figure 3), and developed algorithms and software to conduct measurements during future field campaigns.

We refined the SIT data fusion model, and used it to develop, analyze and compare 5 data processing scenarios (Figures 4,5,6,9, and 16). Within Optech International, the project manager and the software development team adopted the SIT model as a valuable tool to discuss and compare different strategies, and it has proved to be useful for the management of software development. We presented the SIT model at two international remote sensing conferences and discussed its use and value with colleagues in the industry.

We conceived and implemented 3 high-level data fusion algorithms: a Dempster-Shafer algorithm for combining prior classifications from the lidar and spectral data (Figure 6); a procedure to combine blobs extracted separately from the two instruments (Figure 9); and a rule-based decision procedure to combine topographic data (Figure 16).

Using the results shown in Figure 16, we developed a procedure to auto-extract and auto-attribute shoreline vectors (Figures 21, 22, and 23). To support this effort, we developed methods to use the lidar reflectance images to boresight the spectrometer, and this procedure assures the availability of co-registered data.

IMPACT AND APPLICATIONS

National Security

We believe the best strategy for mapping and monitoring the shallow waters and beach areas of the coastal zone is to combine simultaneously-acquired active and passive image data. To date, data fusion strategies for this purpose have been developed in an ad hoc fashion. In this NOPP project, we have developed and implemented the SIT data fusion model, and used it to develop and compare alternate strategies for the combination of active images from the green lidar and passive spectral data from an imaging spectrometer. As anticipated in our original proposal, we have found higher-level data fusion strategies deliver better results for classification purposes.

Economic Development

We believe the new data fusion tools developed in this project will be implemented in commercial airborne remote sensing systems. Also, the collaboration between industry and academia established in this project has led to a more robust collaboration between Optech International and the University of Southern Mississippi forming the basis of a center of expertise in airborne lidar for bathymetric mapping.

Quality of Life

Data fusion techniques developed in this NOPP project should have application to benthic habitat mapping projects designed to map and monitor fish habitat and coral reef health.

Science Education and Communication

Prior to this project, no university in the world had a program of instruction covering bathymetric lidar. Over the past year, USM has integrated bathymetric lidar into its curriculum and into its research. Furthermore, USM's research capabilities in the field of ocean optics have proved valuable in the development of algorithms at Optech International for benthic mapping.

TRANSITIONS

Quality of Life

As part of JALBTCX, the U.S. Army Corps of Engineers and NOAA presently operate an airborne system capable of simultaneously measuring airborne active and passive data. The algorithms and software developed in this NOPP project have been delivered to personnel at JALBTCX.

Science Education and Communication

The data fusion paradigm developed in this partnership, and the datasets have been shared with interested researchers at other universities.

RELATED PROJECTS

Subsequent to the award of this NOPP project, Optech International received a contract from the U.S. Office of Naval Research (ONR) to use bathymetric lidar combined with passive spectral data for seafloor classification as it relates to the detection of mines. This project is named: Counter-mine Lidar UAV-based System (CLUBS). Optech International received a second contract from the U.S. Army Corps of Engineers to develop a new generation of bathymetric lidar systems: the Coastal Zone Mapping and Imaging Lidar (CZMIL). These three projects are distinct, but have some commonality. For example, all three involve collaborations between Optech International and the University of Southern Mississippi. The data fusion paradigm developed in the NOPP project will be used to formulate, present, and quantify the work in CLUBS and CZMIL. A number of personnel at Optech will work on both projects.

REFERENCES

- [1] Pegau, W. S., D. Gray and J. R. Zaneveld (1997). "Absorption and attenuation of visible and near-infrared light in water: dependence on temperature and salinity." *Applied Optics* 36: 6035-6046.
- [2] Zaneveld, J. R. V., J. C. Kitchen and C. Moore (1994). "Scattering correction of reflecting tube absorption meter." *Proceedings of the Society of Photo-Optical Instrumentation Engineers* 2258: 44-55.
- [3] Sogandares, F. M. and E. S. Fry(1997). "Absorption spectrum (340-640nm) of pure water. I. Photothermal measurements," *Appl. Opt.*, 36, 8699--8709
- [4] Pope, R. M. and E. S. Fry (1997) "Absorption spectrum (380-700nm) of pure water. II. Integrating cavity measurements," *Appl. Opt.*, 36, 8710—8723
- [5] Buiteveld, H. et al. (1994) The optical properties of pure water, in *Ocean Optics XII*, J.S.Jaffe, ed., *Proc SPIE* 2258: 174-183 (Table 1)
- [6] Twardowski, M. S., E. Boss, J. B. Macdonald, W. S. Pegau, A. H. Barnard, and J. R. V. Zaneveld (2001), A model for estimating bulk refractive index from the optical backscattering ratio and the implications for understanding particle composition in case I and case II waters, *Journal of Geophysical Research*, 106, 14129.
- [7] Mobley, C. D. (1994). *Light and Water. Radiative Transfer in Natural Waters*. San Diego, CA, Academic Press.

[8] Tuell, G., and J.Y. Park, 2004, "Use of SHOALS Bottom Reflectance Images to Constrain the Inversion of a Hyperspectral Radiative Transfer Model", Proc. SPIE Vol. 5412, Laser Radar and technology Applications IX, G. Kammerman Ed., p. 185-193.

[9] Park, J.Y., 2002, *Data Fusion Techniques for Object Space Classification Using Airborne Laser Data and Airborne Digital Photographs*, Ph.D. Dissertation, Department of Civil and Coastal Engineering, Univeristy of Florida, Gainesville, Florida.

[10] Haralick, R.M. and L.G. Shapiro, 1992, *Computer and Robot Vision*, Addison Wesley.

PUBLICATIONS

Park, J.Y. and G. Tuell, 2006, "An Active/Passive Data Fusion Model for Seafloor Imaging and Benthic Mapping", presented at IEEE International Geoscience and Remote Sensing Symposium, Denver, Colorado.